

RESEARCH PAPER



## ATG4B antagonizes antiviral immunity by GABARAP-directed autophagic degradation of TBK1

Weihong Xie<sup>a\*</sup>, Chenqiu Zhang<sup>b\*</sup>, Zheyu Wang<sup>b</sup>, Hui Chen<sup>a</sup>, Tonghui Gu<sup>b</sup>, Tao Zhou<sup>b</sup>, Yaoxing Wu<sup>b</sup>, Fan Xia<sup>b</sup>, Min Li<sup>c</sup>, Jun Wang<sup>d</sup>, Renjie Jiao<sup>a</sup>, Jun Cui<sup>b</sup>, and Shouheng Jin<sup>b</sup>

<sup>a</sup>Sino-French Hoffmann Institute, School of Basic Medical Sciences, Guangzhou Medical University, Guangzhou, Guangdong, China; <sup>b</sup>Guangdong Province Key Laboratory of Pharmaceutical Functional Genes, MOE Key Laboratory of Gene Function and Regulation, State Key Laboratory of Biocontrol, School of Life Sciences, Sun Yat-Sen University, Guangzhou, Guangdong, China; <sup>c</sup>School of Pharmaceutical Sciences, Sun Yat-Sen University, Guangzhou, Guangdong, China; <sup>d</sup>Department of Pediatric Surgery, Guangdong Provincial Key Laboratory of Research in Structural Birth Defect Disease, Guangdong Provincial Clinical Research Center for Child Health, Guangzhou Institute of Pediatrics, Guangzhou Women and Children's Medical Center, Guangzhou Medical University, Guangzhou, China

### ABSTRACT

TBK1 (TANK binding kinase 1) is an essential kinase of antiviral immunity, yet the regulatory mechanisms responsible for its stringent control via autophagy are not fully understood. Here, we identify the macroautophagy/autophagy-related cysteine protease ATG4B as a negative regulator of human antiviral immune responses by targeting TBK1 for autophagic degradation at the advanced stage of viral infection. Mechanistically, ATG4B serves as an adaptor for recruiting TBK1 to GABARAP (GABA type A receptor-associated protein), which subsequently leads to the TBK1-GABARAP interaction through the LC3-interacting region (LIR) motif of TBK1 ULD domain. Moreover, pharmacological ATG4B inhibitor, a small molecule named S130, contributes to host defense against viral infection and blocks ATG4B-dependent autophagic degradation of TBK1. Accordingly, S130 increases antiviral response and inhibits the VSV infection both *in vitro* and *in vivo*. Altogether, our study reveals the regulatory role of ATG4B in modulating TBK1-centered type I interferon (IFN) signaling, and indicates that ATG4B suppression can provide a potential therapy target for viral infection.

**Abbreviations:** Baf A<sub>1</sub>: bafilomycin A<sub>1</sub>; GABARAP: GABA type A receptor-associated protein; GFP: green fluorescent protein; IFN: interferon; IKBKE/IKKi: inhibitor of nuclear factor kappa B kinase subunit epsilon; IRF3: interferon regulatory factor 3; ISG: interferon-stimulated gene; ISRE: IFN-stimulated response element; MAP1LC3/LC3: microtubule associated protein 1 light chain 3; MAVS: mitochondrial antiviral signaling protein; MOI: multiplicity of infection; PAMPs: pathogen-associated molecule patterns; RIGI/DDX58: RNA sensor RIG-I; SeV: Sendai virus; siRNA: small interfering RNA; TBK1: TANK binding kinase 1; WT: wild-type; VSV: vesicular stomatitis virus.

### ARTICLE HISTORY

Received 3 November 2022  
Revised 15 June 2023  
Accepted 3 July 2023

### KEYWORDS

Antiviral immune response;  
ATG4B; LC3-interacting  
region; selective autophagy;  
TBK1



### Introduction

To restrict the invasion of viral pathogens, the innate immune system initiates antiviral responses and provides the first line of host defense through detecting pathogen-associated molecular patterns (PAMPs) [1]. During viral infection, the pattern recognition receptors (PRRs) recognize the viral PAMPs and facilitate the signaling cascades leading to the production of pro-inflammatory cytokines and type I interferons (IFNs) [2]. Subsequently, type I IFNs induce the synthesis of restriction factors to eliminate the invading virus and provoke comprehensive host defenses [3].


TBK1 (TANK binding kinase 1) is an essential kinase for type I IFNs production. Upon viral infection, TBK1 is activated and triggers the phosphorylation and translocation of IRF3 (interferon regulatory factor 3), which then initiates the production of IFNs and other pro-inflammatory cytokines [4]. The activation of TBK1 is strictly orchestrated by multiple

post-transcriptional mechanisms, including phosphorylation, ubiquitination, SUMOylation, and acetylation [5–7]. In Addition, the stability of TBK1 is tightly controlled to maintain its function by ubiquitin-proteasome system and lysosome-dependent system [8–12]. TBK1 could be sequestered into lysosomes for degradation via chaperone-mediated autophagy/CMA [12]. Moreover, we recently demonstrated that ubiquitinated TBK1 could be recognized by the cargo receptor CALCOCO2/NDP52 and selectively delivered to autophagosomes for degradation during viral infection [11]. However, the regulatory mechanisms of autophagic degradation of TBK1 are still not well understood.

Macroautophagy/autophagy is an evolutionarily conserved process, which degrades the damaged proteins, unwanted organelles and invading microbial pathogens and plays a fundamental role in maintaining the intracellular homeostasis [13]. Dysfunctional autophagy pathway

**CONTACT** Shouheng Jin  [jinshh3@mail.sysu.edu.cn](mailto:jinshh3@mail.sysu.edu.cn)  Guangdong Province Key Laboratory of Pharmaceutical Functional Genes, MOE Key Laboratory of Gene Function and Regulation, State Key Laboratory of Biocontrol, School of Life Sciences, Sun Yat-sen University, Guangzhou, Guangdong 510275, China  
This article has been corrected with minor changes. These changes do not impact the academic content of the article.

\*These authors contributed equally to this work.

 Supplemental data for this article can be accessed online at <https://doi.org/10.1080/15548627.2023.2233846>

is often manifested as a variety of diseases, including liver diseases, metabolic disorders, cancers, autoimmunity, neurodegeneration, and infectious diseases [14,15]. Accumulating evidence has shown that autophagy is crucial for antiviral defense [16]. On the one hand, autophagy is a power tool in antiviral defense by degrading viruses and viral components [17]. On the other hand, autophagy prevents the host from pathology by suppressing the components of immune factors [15]. However, autophagy might be hijacked by enterovirus and enterovirus benefits from autophagy for its replication in infected cells [18]. Poliovirus, a well-known enterovirus, induces autophagy to form a double-membrane vesicle for its viral RNA replication. The proteins 2BC and 3A of poliovirus increase LC3 lipidation and the formation of double-membrane vesicle [19,20].

Autophagy is orchestrated by a number of evolutionarily conserved autophagy-related (ATG) proteins [13]. The ATG4-Atg8-family protein ubiquitin-like conjugation system is vital for expansion of phagophores [21]. ATG4, as a cysteine protease, contributes to Atg8-family protein lipidation by cleaving the C terminus amino acid of cytoplasmic Atg8-family protein precursors [22]. In mammalian cells, there are four orthologs of ATG4 (ATG4A, ATG4B, ATG4C, and ATG4D), encoded by four independent genes [23]. ATG4B is the main isoform of ATG4 by presenting the most remarkable activity than others [24]. Defective autophagy caused by genetic inhibition or inborn errors of immunity of *ATG4A* and *LC3B2* in humans results in increased HSV-2 replication in model systems and cells from patients with recurrent lymphocytic HSV-2 Mollaret meningitis [25]. ATG4B helps enterovirus 71 (EV71) replication through hydrolytically processing the polyprotein of EV71 [26]. These results suggest that ATG4 family members might play critical roles in antiviral defense. However, the underlying mechanism of ATG4 orthologs modulating the host antiviral immunity remains unclear and requires further investigation.

Here, we found that ATG4B serves as a negative regulator in human antiviral immune responses by targeting TBK1 in the advanced stage of viral infection, and serves as an adaptor bridging TBK1 to GABARAP (GABA type A receptor-associated protein), an Atg8-family protein belonging to GABARAP subfamily. Mechanistically, GABARAP binds to the LIR motif present in ULD domain of TBK1, leading to TBK1-GABARAP interaction for further autophagic degradation. Moreover, a small molecule S130, strongly suppressing the cleavage activity of ATG4B, blocks ATG4B-dependent autophagic degradation of TBK1 and contributes to the host defense against viral infection. S130 was further shown to increase antiviral response and attenuate VSV infection *in vitro* and *in vivo*. Therefore, our findings demonstrate that ATG4B plays an essential role in TBK1-centered antiviral immunity and prevents the host from excessive immune responses. In addition, the ATG4B inhibitor S130 can be a potential therapeutic reagent against virus infection and insufficient immune responses.

## Results

### *ATG4B* negatively regulates type I IFN signaling

Accumulating evidence indicates that antiviral immunity is modulated by autophagy, as well as the ATGs [27]. To investigate the effect of ATG4 on antiviral immunity, we performed luciferase reporter assay and found that the activation of IFN-stimulated response element (ISRE) induced by Sendai virus (SeV) was suppressed by ectopic expression of ATG4B, but not other orthologs of ATG4, such as ATG4A, ATG4C or ATG4D (Figure S1A). Next, we efficiently knocked out *ATG4B* in 293T cells (Figure S1B) and confirmed that *ATG4B* depletion could significantly increase the activation of ISRE by infection of SeV and intracellular (IC) poly (I:C) treatment with different time points (Figure 1A). We moved on to observe that *ATG4B* deficiency remarkably increased the phosphorylation of IRF3 (Figure 1B and S1C). To further characterize the role of ATG4B under physiological conditions, we efficiently knocked down *ATG4B* in THP-1-derived macrophages (Figure S1D) and enhanced phosphorylation of IRF3 was observed in *ATG4B*-depleted THP-1-derived macrophages upon SeV infection (Figure S1E and S1F). Meanwhile, we obtained similar results in *ATG4B*-deficient human peripheral blood mononuclear cells (PBMCs) during influenza A virus H1N1 infection (Figure 1C and S1G). Additionally, quantitative RT-PCR analyses showed that the *ATG4B* deficiency resulted in more *IFIT2/ISG54*, *IFIT1/ISG56* and *IFNB1* mRNA than control cells during SeV infection (Figure 1D and S1H). *ATG4B*-deficient PBMCs also showed more *IFIT2/ISG54*, *IFIT1/ISG56* and *IFNB1* mRNA than control cells during H1N1 infection (Figure 1E). To observe vesicular stomatitis virus (VSV) replication in cells, we infected A549 cells with GFP-tagged VSV. Fluorescence microscopy analyses showed a significant decrease fluorescence intensity in *ATG4B*-deficient cells than control cells (Figure 1F). Meanwhile, flow cytometry analyses showed that the percentage of GFP<sup>+</sup> (virus-infected) cells was considerably decreased in *ATG4B*-deficient cells compared with control cells (Figure 1G). Collectively, these results suggest that ATG4B negatively regulates type I IFN signaling as well as antiviral immunity.

### *ATG4B* interacts with TBK1

To explore the molecular target of ATG4B in type I IFN signaling, we performed luciferase reporter assay and found that ATG4B inhibited the activation of luciferase reporter, as well as *IFIT2/ISG54*, *IFIT1/ISG56* and *IFNB1* expression, induced by RIGI/DDX58, IFIH1/MDA5, MAVS and TBK1, but not IKBKE/IKKi or IRF3 (5D) (a constitutively active mutant of IRF3) (Figure 2A and S2A). Subsequently, we investigated whether ATG4B regulates type I IFN signaling via targeting TBK1. Coimmunoprecipitation assay revealed that endogenous association between ATG4B and TBK1 in A549 cells was remarkably increased during SeV infection, especially in the later stage of viral infection (Figure 2B and S2B). Similar result was obtained in THP-1-derived macrophages infected with SeV (Figure 2C and S2C). Further confocal microscopy analyses showed that some of ATG4B and

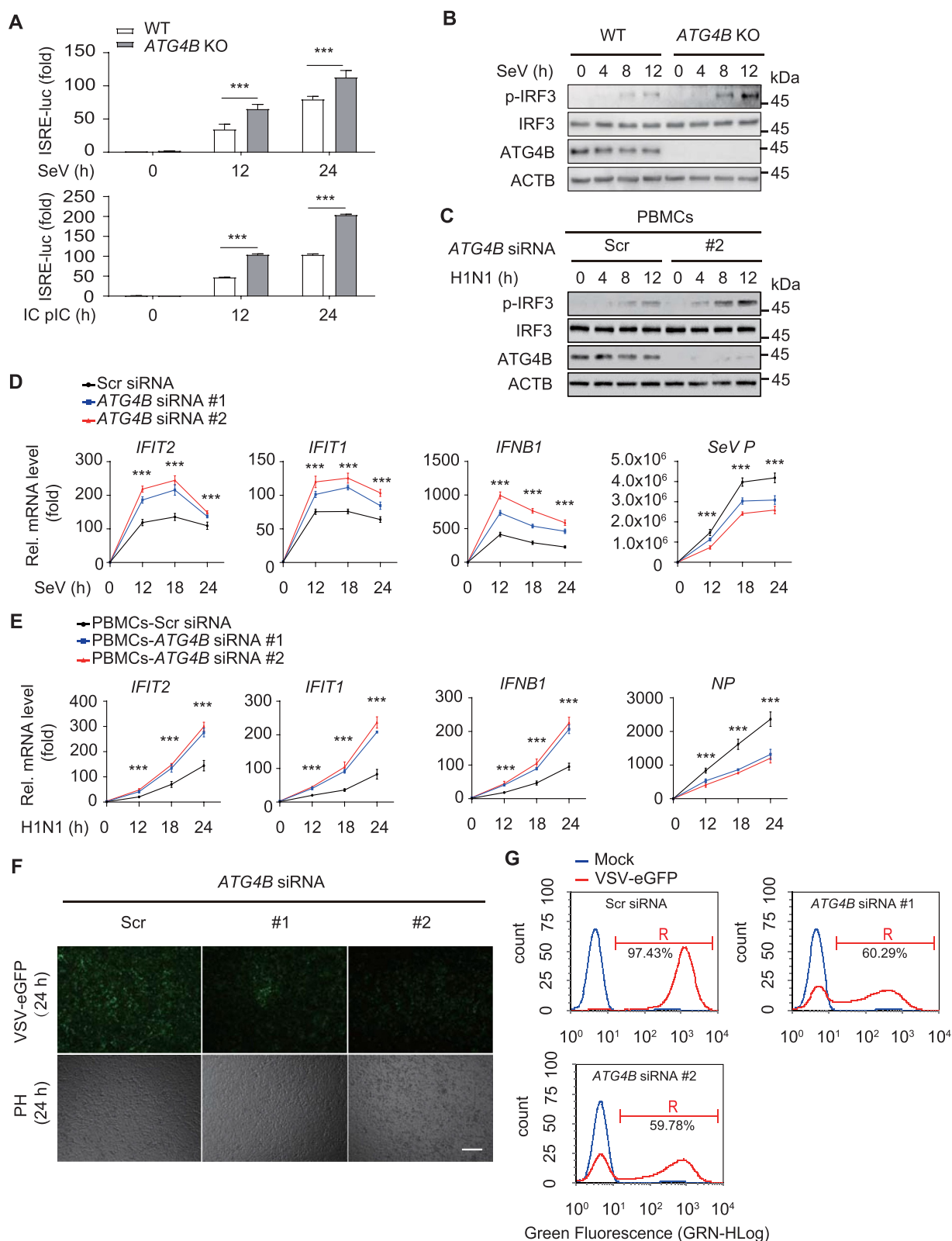


**Figure 1.** ATG4B negatively regulates type I IFN signaling. **(A)** Luciferase activity in wild-type (WT) or *ATG4B* knockout (KO) 293T cells transfected with an ISRE luciferase reporter (ISRE-luc), followed by treatment with or without SeV (MOI = 0.1) or intracellular (IC) poly (I: C) (5  $\mu$ g/mL) infection at the indicated time points, respectively. **(B)** WT or *ATG4B* KO 293T cells were treated with or without SeV (MOI = 0.1) infection at indicated time points. Protein lysates were immunoblotted with indicated antibodies. **(C)** Human peripheral blood mononuclear cells (PBMCs) were transfected with scrambled (Scr) siRNA or *ATG4B* siRNA, followed by treatment with or without H1N1 (MOI = 1) infection at indicated time points. Protein lysates were immunoblotted with indicated antibodies. **(D)** Quantitative RT-PCR analyses of indicated gene expression in A549 cells transfected with Scr siRNA or *ATG4B* siRNA, followed by treatment with or without SeV (MOI = 0.1) infection at indicated time points. **(E)** Quantitative RT-PCR analyses of indicated gene expression in PBMCs transfected with Scr siRNA or *ATG4B* siRNA, followed by treatment with or without H1N1 (MOI = 1) infection at indicated time points. **(F and G)** Phase-contrast (PH) and fluorescence microscopy analyses (F) or flow cytometry analyses (G) of A549 cells transfected with Scr siRNA or *ATG4B* siRNA treated with VSV-eGFP (MOI = 0.01) infection for 24 h. Scale bars: 200  $\mu$ m. In (A, D and E), all error bars, mean values  $\pm$  SEM, *P*-values were determined by unpaired two-tailed Student's *t* test of *n* = 3 independent biological experiments, \*\*\* *P* < 0.001. For (B, C, F and G), similar results are obtained from three independent biological experiments.

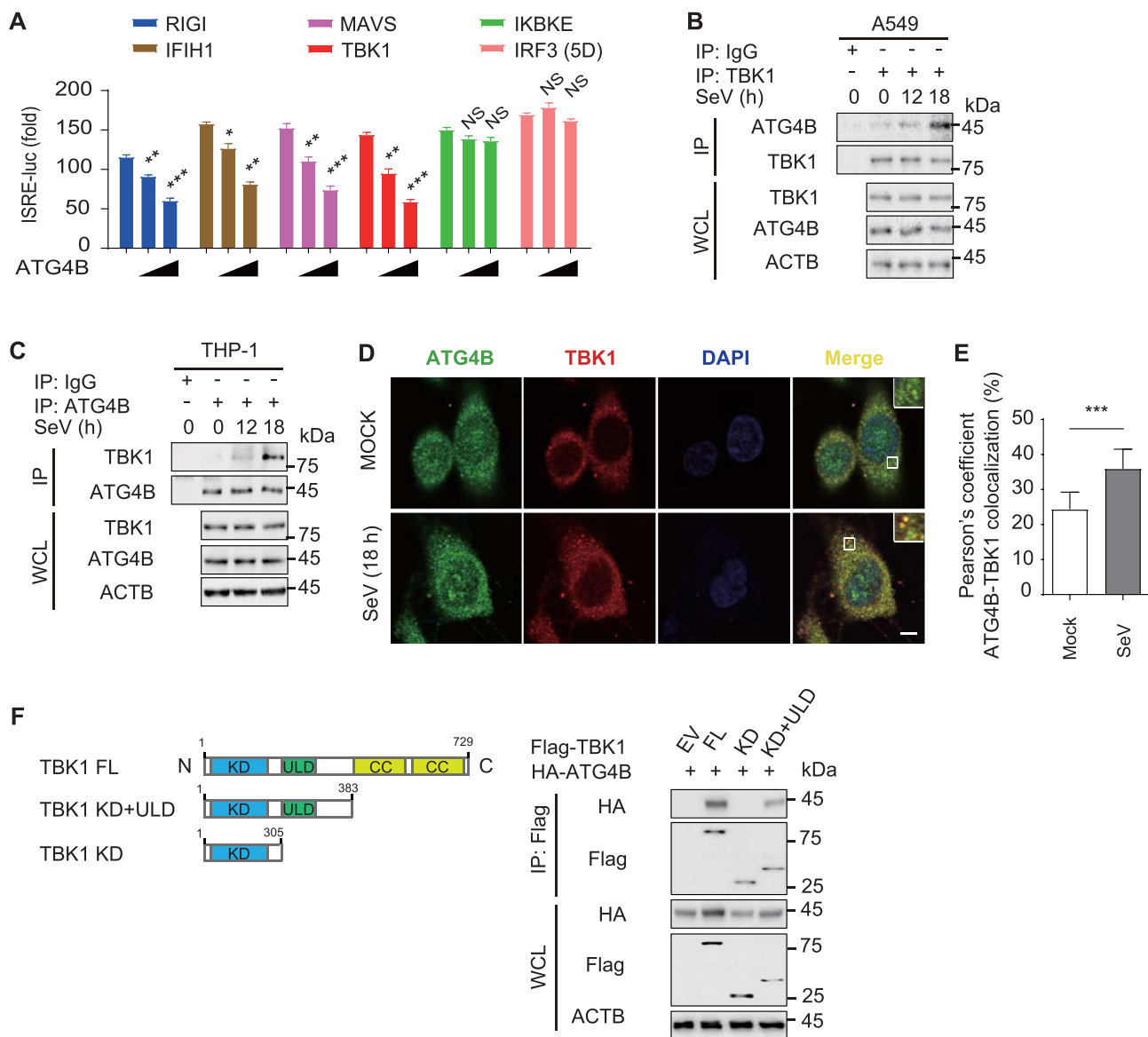


**Figure 2.** ATG4B interacts with TBK1. **(A)** Luciferase activity in 293T cells transfected with an ISRE luciferase reporter (ISRE-luc), together with the indicated plasmids along with empty vector (EV) or increasing amounts (wedge) of expression vector for HA-ATG4B. **(B)** Protein lysates of A549 cells infected with SeV (MOI=0.1) for indicated time points were immunoprecipitated with anti-TBK1 antibody and immunoblot analyses with indicated antibodies. **(C)** Protein lysates of THP-1-derived macrophages infected with SeV (MOI=0.1) for indicated time points were immunoprecipitated with anti-ATG4B antibody and immunoblot analyses with indicated antibodies. **(D and E)** A549 cells were treated with SeV (MOI=0.1) infection for 18 h. Confocal microscopy **(D)** by labeling of ATG4B and TBK1 with specific primary antibody and Alexa Fluor 488 goat anti-Rabbit IgG (H+L) (green) or CF568 donkey anti-goat-IgG secondary antibody (red). Scale bars: 20  $\mu$ m. Quantitative analyses **(E)** of the colocalization (30 cells per group). Data are expressed as means  $\pm$  SD of 30 cells. **(F)** Coimmunoprecipitation and immunoblot analyses of 293T cells transfected with vectors for TBK1 and its deletions along with vector encoding HA-ATG4B. In **(A)**, all error bars, mean values  $\pm$  SEM, *P*-values were determined by unpaired two-tailed Student's *t* test of *n* = 3 independent biological experiments, \**P* < 0.05, \*\**P* < 0.01 and \*\*\* *P* < 0.001. NS: not significant. For **(B-F)**, similar results are obtained from three independent biological experiments.

TBK1 expressed at the same location in uninfected A549 cells, and the colocalization between ATG4B and TBK1 was enhanced upon SeV infection (Figure 2D,E). Next, we constructed two truncated TBK1 mutants to explore which domain(s) interact with ATG4B. Immunoblot analyses revealed that ATG4B could interact with TBK1 mutant containing the kinase domain (KD) and ubiquitin-like domain (ULD), but not the mutant containing only KD domain, suggesting that ULD domain of TBK1 is required for its association with ATG4B (Figure 2F). Taken together, these results reveal that ATG4B inhibits type I IFN signaling by targeting TBK1.

### ATG4B promotes the autophagic degradation of TBK1

To further characterize the inhibitory function of ATG4B in type I IFN signaling through its association with TBK1, we examined the effect of ATG4B on the stability of TBK1. Immunoblot analyses demonstrated that the increasing amount of ATG4B markedly decreased the protein level of TBK1 (Figure 3A and S3A). Further quantitative RT-PCR analyses revealed that the increasing amount of ATG4B resulted in unchanged abundance of *TBK1* mRNA (Figure 3B), suggesting that ATG4B promotes TBK1 protein degradation. Subsequently, immunoblot analyses revealed that



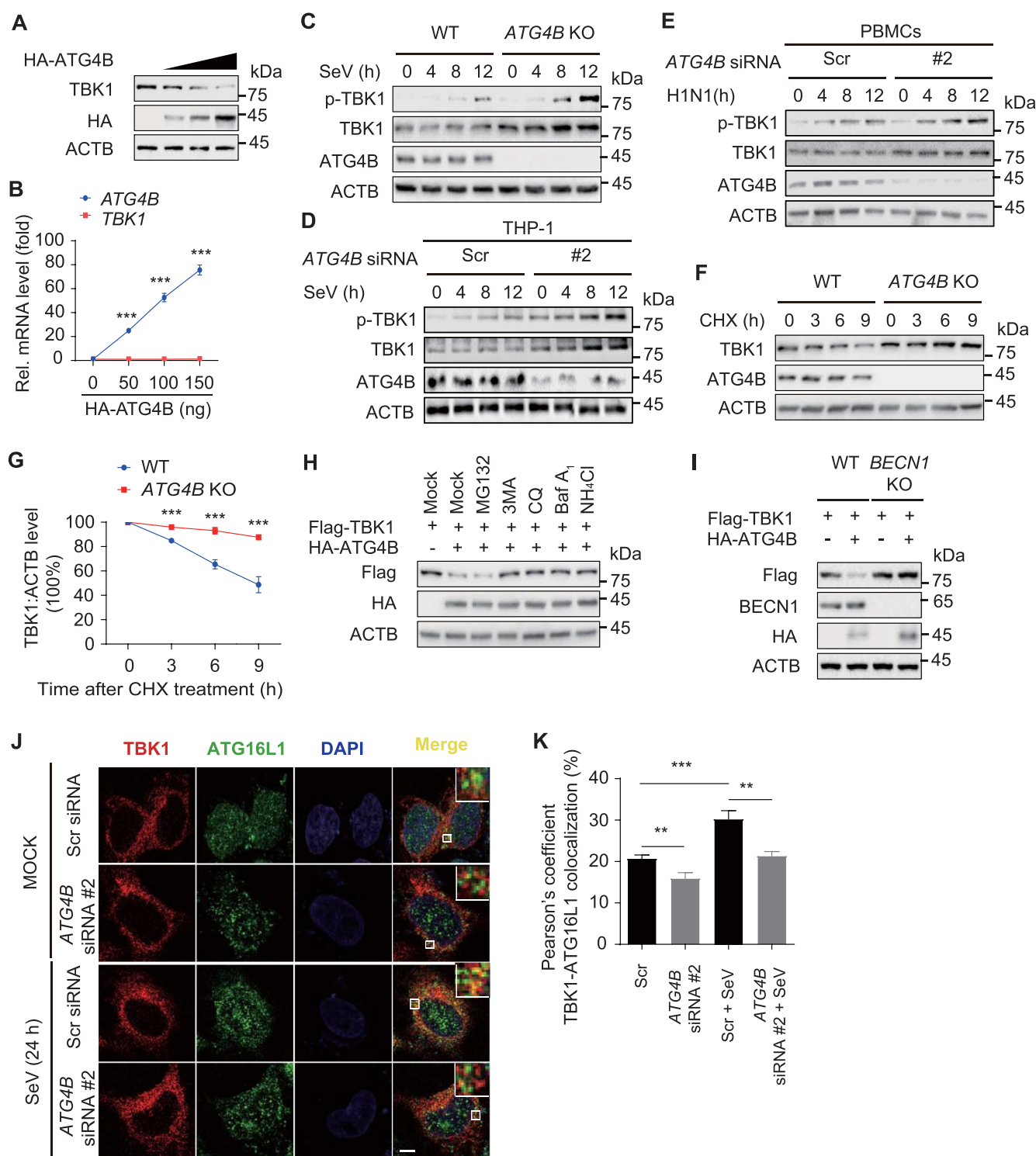


**Figure 3.** ATG4B promotes the autophagic degradation of TBK1. (A) 293T cells were transfected with vector for Flag-TBK1, together with increasing amounts (wedge) of expression vector for HA-ATG4B, and the protein was harvested for immunoblot analyses. (B) Quantitative RT-PCR analyses of *ATG4B* mRNA and *TBK1* mRNA in (A). (C) Protein lysates of wild-type (WT) and *ATG4B* knockout (KO) 293T cells infected with SeV (MOI = 0.1) at indicated time points were immunoblotted with indicated antibodies. (D) THP-1-derived macrophages were transfected with scrambled (Scr) siRNA or *ATG4B* siRNA, followed by SeV (MOI = 0.1) infection for indicated time, the lysates were then analyzed with indicated antibodies. (E) Human peripheral blood mononuclear cells (PBMCs) were transfected with Scr siRNA or *ATG4B* siRNA, followed by H1N1 (MOI = 1) infection for indicated time, the lysates were then analyzed with indicated antibodies. (F) Protein lysates of WT and *ATG4B* KO 293T cells treated with cycloheximide (CHX) (100  $\mu$ g/mL) for the indicated time points were immunoblotted with the indicated antibodies. (G) Quantification of the expression levels of TBK1 shown in (F). (H) 293T cells were transfected with vector for Flag-TBK1, together with the plasmids encoding empty vector (EV) or HA-ATG4B. Protein lysates of the cells treated with MG132 (10  $\mu$ M), 3 MA (10 mM), CQ (50  $\mu$ M), bafilomycin A<sub>1</sub> (Baf A<sub>1</sub>) (0.2  $\mu$ M) and NH<sub>4</sub>Cl (20 mM) for 6 h respectively, were immunoblotted with the indicated antibodies. (I) Protein lysates of WT and *BECN1* KO 293T cells transfected with vector for Flag-TBK1, together with the plasmids encoding EV or HA-ATG4B, were immunoblotted with indicated antibodies. (J and K) A549 cells were transfected with Scr siRNA or *ATG4B* siRNA, followed by treatment with SeV (MOI = 0.1) infection for 24 h. Confocal microscopy (J) by labeling of TBK1 and ATG16L1 with specific primary antibody and Alexa Fluor 488 goat

*ATG4B*-deficient cells present an increase in the protein abundance of TBK1 both in un-infected and SeV-infected cells (Figure 3C and S3B). Furthermore, we knocked down *ATG4B* in THP-1-derived macrophages and PBMCs and found that *ATG4B* depletion resulted in increased protein levels of TBK1 both in un-infected and SeV or H1N1-infected cells (Figure 3D,E and S3C, S3D). Next, *ATG4B* depletion slowed the clearance of TBK1 in cycloheximide (CHX) treated cells (Figure 3F,G). To figure out which degradation system involves in *ATG4B*-mediated TBK1 degradation, ubiquitin-proteasome inhibitor and autophagy inhibitors were used and immunoblot analyses showed the degradation of TBK1 induced by *ATG4B* was blocked by 3-methyladenine (3 MA), chloroquine (CQ), bafilomycin A<sub>1</sub> (Baf A<sub>1</sub>) and NH<sub>4</sub>Cl, but not the proteasome inhibitor MG132 treatment (Figure 3H and S3E). Moreover, the degradation of TBK1 mediated by *ATG4B* was almost abrogated in *BECN1* knockout cells (Figure 3I and S3F). Likewise, confocal microscopy analyses revealed that TBK1 interacted with ATG16L1, which plays a critical role in Atg8-family protein lipidation and elongation of autophagosome, and *ATG4B* deficiency decreased the colocalization between TBK1 and ATG16L1 (Figure 3J,K). Altogether, these results suggest that *ATG4B* promotes the autophagic degradation of TBK1.

#### ***ATG4B* promotes TBK1 degradation through GABARAP**

Since *ATG4B* and ATG16L1 are vital for Atg8-family protein lipidation, as well as elongation of nascent autophagosomes, we next asked whether *ATG4B* has effect on TBK1 via Atg8-family proteins. Coimmunoprecipitation and immunoblot analyses showed that TBK1 could interact with LC3 (MAP1LC3A, MAP1LC3B, MAP1LC3C) and GABARAP (GABARAP, GABARAPL1, GABARAPL2), while among them, the interaction between TBK1 and GABARAP was the strongest (Figure 4A). Moreover, *ATG4B* could markedly increase the association between TBK1 and GABARAP (Figure 4B and S4A), whereas *ATG4B* deficiency abrogated the endogenous association between TBK1 and GABARAP (Figure 4C and S4B). To further confirm the role of *ATG4B* in the association between TBK1 and GABARAP, THP-1-derived macrophages infected with SeV at different time points were immunoprecipitated. We observed that *ATG4B* strongly interacted with TBK1 at 18 h post-SeV infection, while the apparent association between TBK1 and GABARAP could be detected at a later time point (around 24 h post infection), which revealed the dynamic assembly of the *ATG4B*-TBK1-GABARAP complex (Figure 4D and S4C). These results suggest that *ATG4B* function as a scaffold for recruiting TBK1 to GABARAP and *ATG4B* is indispensable for TBK1-GABARAP association. Next, we substantiated

whether GABARAP involves in *ATG4B*-mediated TBK1 autophagic degradation. Indeed, *ATG4B* failed to promote the degradation of TBK1 in *GABARAP* knockout cells (Figure 4E and S4D). Similarly, *GABARAP* depletion slowed the clearance of TBK1 in CHX-treated cells (Figure 4F, G). Luciferase reporter assay indicated that *ATG4B* failed to inhibit the activation of TBK1-centered type I IFN signaling in *GABARAP*-deficient cells (Figure 4H). Collectively, these results suggest that *ATG4B* promotes the autophagic degradation of TBK1 via GABARAP.

As Atg8-family protein proteolytic activation is regulated by *ATG4*, which cleaves cytoplasmic Atg8-family protein to expose a C-terminal glycine residue required for Atg8-family protein lipidation. Afterwards, Atg8-family protein is covalently conjugated to membrane-bound phosphatidylethanolamine (PE) through its C-terminal glycine residue for expansion of nascent autophagosomes [21]. To further investigate whether *ATG4B* regulates TBK1 stability via its function on Atg8-family protein processing, we generated *GABARAP* uncleavable mutant (*GABARAP*<sup>G116A</sup>) and truncated C-terminal mutant of *GABARAP* (*GABARAP* [ΔC]), which lacks Leu117 (Figure 4I and S4E) [24,28]. However, we found that *GABARAP*<sup>G116A</sup> and *GABARAP* [ΔC] mutants could interact with TBK1, as well as wild-type (WT) *GABARAP*, in wild-type 293T cells, but not in *ATG4B*-deficient cells (Figure S4F, S4G). These results demonstrate that the cleavage of *GABARAP* is not essential for its interaction with TBK1.

Further immunoblot analyses showed that overexpression of WT *GABARAP*, but not *GABARAP*<sup>G116A</sup> mutant, resulted in modestly decreased TBK1, while *GABARAP* [ΔC] mutant could markedly promote the degradation of TBK1 in WT 293T cells (Figure 4J and S4H). However, overexpression of *GABARAP* [ΔC] mutant, as well as WT *GABARAP* or *GABARAP*<sup>G116A</sup> mutant, failed to induce significant TBK1 degradation in *ATG4B*-deficient cells, revealing that *ATG4B* was required for *GABARAP*-mediated TBK1 degradation. Likewise, luciferase reporter assays also indicated that overexpression of *GABARAP* [ΔC] mutant, but not the WT *GABARAP* and *GABARAP*<sup>G116A</sup> mutant, could inhibit the activation of TBK1-centered type I IFN signaling in WT 293T cells (Figure 4K). These results demonstrate that *ATG4B* is indispensable for *GABARAP*-TBK1 interaction and *ATG4B*-mediated *GABARAP* cleavage is essential for the autophagic degradation of TBK1.

#### ***LIR* motif of TBK1 is required for its interaction with GABARAP**

To discover the mechanism by which *ATG4B* regulates TBK1 degradation via *GABARAP*, we assessed the effect of *ATG4B* in

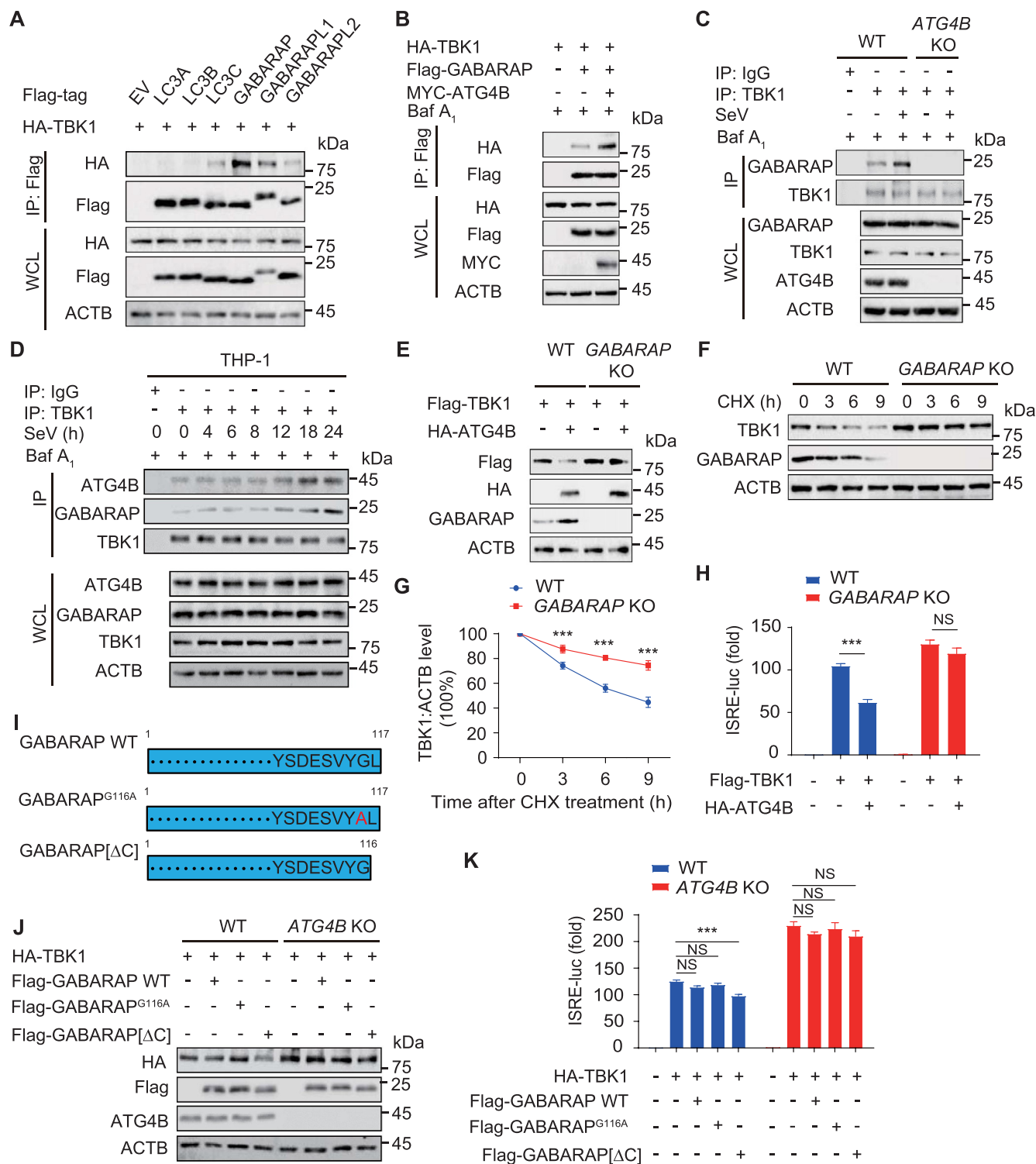


**Figure 4.** ATG4B promotes TBK1 degradation through GABARAP. **(A)** 293T cells were transfected with vector encoding HA-TBK1, together with Flag-tagged Atg8 family members. Protein lysates were harvested for immunoprecipitation with anti-Flag beads and immunoblot analyses with anti-HA. **(B)** 293T cells were transfected with vectors encoding HA-TBK1 and Flag-GABARAP, together with MYC-ATG4B. Protein lysates were harvested after bafilomycin A<sub>1</sub> (Baf A<sub>1</sub>) (0.2 μM) treatment (6 h) for immunoprecipitation with anti-Flag beads and immunoblot analyses with anti-HA. **(C)** Wild-type (WT) and ATG4B knockout (KO) 293T cells were treated with SeV (MOI=0.1) infection for 18 h. Protein lysates were harvested after Baf A<sub>1</sub> (0.2 μM) treatment (6 h) for immunoprecipitation and immunoblot using indicated antibodies. **(D)** THP-1-derived macrophages were infected with SeV (MOI=0.1) at indicated time points. Protein lysates were harvested after Baf A<sub>1</sub> (0.2 μM) treatment (6 h) for immunoprecipitation with anti-Flag beads and immunoblot analyses with indicated antibodies. **(E)** Protein lysates of WT and GABARAP KO 293T cells transfected with vector for Flag-TBK1, together with the plasmids encoding empty (EV) or HA-ATG4B, were immunoblotted with indicated antibodies. **(F)** Protein lysates of WT and GABARAP KO 293T cells treated with cycloheximide (CHX) (100 μg/mL) for the indicated time points were immunoblotted with the indicated antibodies. **(G)** Quantification of the expression levels of TBK1 shown in (F). **(H)** Luciferase activity in WT or GABARAP KO 293T cells transfected with an ISRE luciferase reporter (ISRE-luc), together with vector for Flag-TBK1 along with EV or expression vector for HA-ATG4B. **(I)** Schematic diagram of GABARAP<sup>G116A</sup> and GABARAP[ΔC] mutants. **(J)** WT or ATG4B KO 293T cells were transfected with vectors for WT GABARAP, GABARAP<sup>G116A</sup> and GABARAP[ΔC] mutants, along with vector encoding HA-TBK1. Different amounts of plasmids for WT GABARAP, GABARAP<sup>G116A</sup> and GABARAP[ΔC] mutants were transfected into cells for equal expression in WT 293T cells. Protein lysates were immunoblotted with indicated antibodies. **(K)** Luciferase activity in WT or ATG4B KO 293T cells transfected with an ISRE-luc, together with vectors for WT GABARAP, GABARAP<sup>G116A</sup> and GABARAP[ΔC] mutants, along with vector encoding HA-TBK1. In (G, H and K), all error bars, mean values ± SEM, *P*-values were determined by unpaired two-tailed Student's *t* test of *n* = 3 independent biological experiments, \*\*\* *P* < 0.001. NS: not significant. For (A-F, J), similar results are obtained from three independent biological experiments.

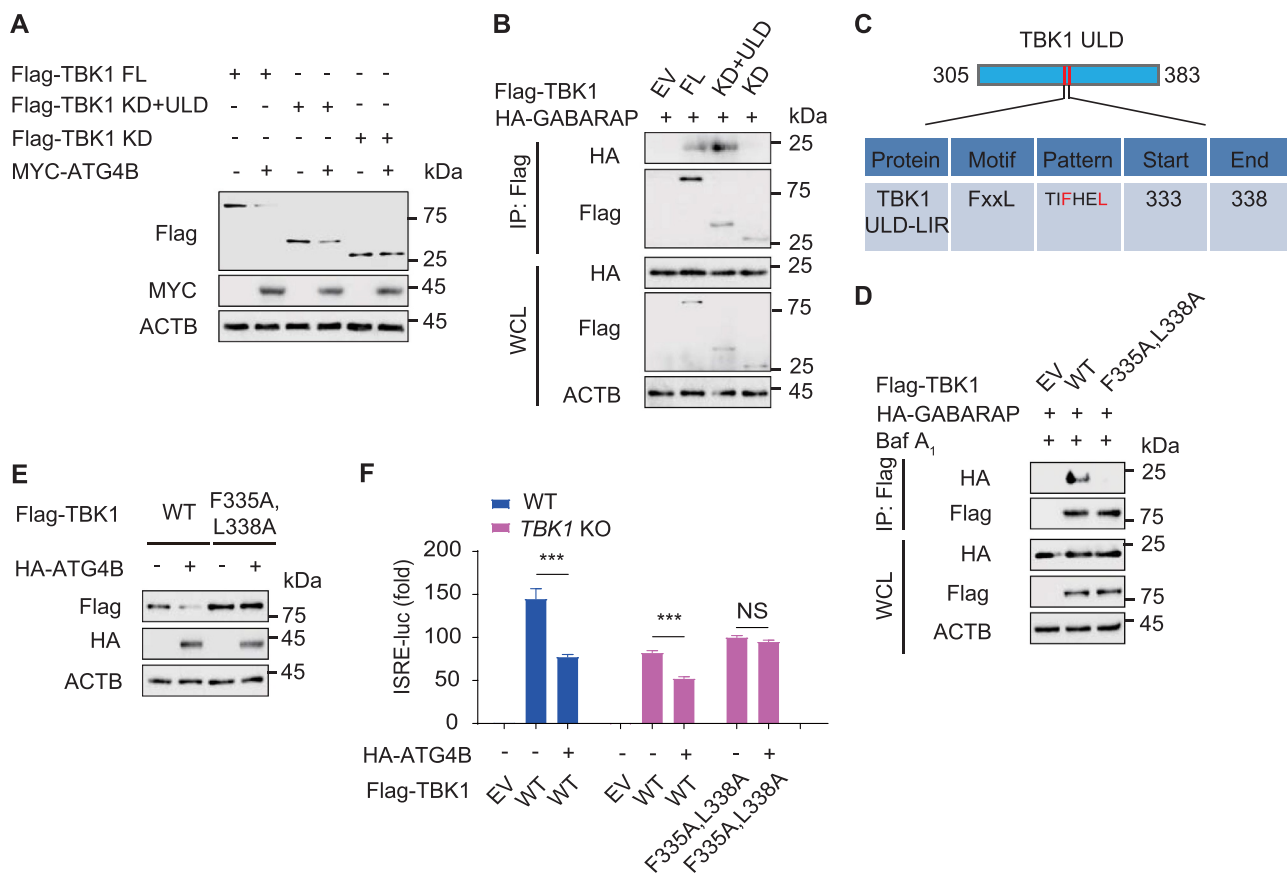


**Figure 5.** LIR motif of TBK1 is required for its interaction with GABARAP. **(A)** Immunoblot analyses of protein extracts of 293T cells transfected with wild-type (WT) or deletion mutants of Flag-TBK1 plasmids, together with empty vector (EV) or expression vector for MYC-ATG4B. **(B)** 293T cells were transfected with WT or deletion mutants of Flag-TBK1 plasmids, together with vector for HA-GABARAP. Protein lysates were harvested for immunoprecipitation with anti-Flag beads and immunoblot analyses with anti-HA. **(C)** Schematic diagram of LIR motif for TBK1 ULD domain. **(D)** 293T cells were transfected with vectors for WT Flag-TBK1 or TBK1<sup>F335A,L338A</sup> mutant, together with plasmid encoding HA-GABARAP. Protein lysates were harvested for immunoprecipitation and immunoblot using indicated antibodies. **(E)** 293T cells were transfected with vectors for WT Flag-TBK1 or TBK1<sup>F335A,L338A</sup> mutant, together with plasmid encoding HA-ATG4B. Protein lysates were harvested for immunoblot analyses with the indicated antibodies. **(F)** Luciferase activity in WT or TBK1 KO 293T cells transfected with an ISRE luciferase reporter (ISRE-luc), together with vectors for WT Flag-TBK1 or TBK1<sup>F335A,L338A</sup> mutant along with EV or expression vector for HA-ATG4B. In **(F)**, all error bars, mean values  $\pm$  SEM, *P*-values were determined by unpaired two-tailed Student's *t* test of *n* = 3 independent biological experiments, \*\*\* *P* < 0.001. NS: not significant. For **(A)**, **(B)**, **(D)** and **(E)**, similar results are obtained from three independent biological experiments.

WT TBK1 and its truncation mutants. We found that ATG4B could promote the degradation of TBK1 mutant containing the KD domain and ULD domain, but not the mutant harboring only KD domain (Figure 5A and S5A). Coimmunoprecipitation and immunoblot analyses showed that GABARAP could interact with TBK1 mutant containing KD and ULD domains, but not the mutant harboring only KD domain (Figure 5B). These results revealed that ULD domain of TBK1 is crucial for ATG4B-mediated TBK1 degradation via GABARAP.

To gain insight into the mechanism of GABARAP in TBK1 autophagic degradation, we performed amino acid sequence analyses and found that the ULD domain of TBK1 exhibits a LIR motif (TIFHEL) (Figure 5C). As the LIR-motif is vital for the interaction between the cargoes and Atg8-family proteins, we constructed a TBK1 ULD-LIR mutant, TBK1<sup>F335A,L338A</sup>. Coimmunoprecipitation and immunoblot analyses showed that the TBK1<sup>F335A,L338A</sup> mutant failed to interact with GABARAP (Figure 5D), suggesting that TBK1 might interact with GABARAP through its LIR motif. Further immunoblot analyses

revealed that ATG4B could not promote the degradation of TBK1<sup>F335A,L338A</sup> mutant (Figure 5E and S5B). Moreover, luciferase reporter assay indicated that ATG4B failed to inhibit the activation of luciferase reporters mediated by TBK1<sup>F335A,L338A</sup> (Figure 5F). These results suggest that the LIR motif of TBK1 ULD domain is essential for ATG4B to promote TBK1 degradation through GABARAP.

Previously we demonstrated that cargo receptor CALCOCO2/NDP52 mediates the selective autophagic degradation of ubiquitinated TBK1 [11]. We next sought to explore whether CALCOCO2 and GABARAP cooperate to orchestrate TBK1 stability. We performed immunoprecipitation and found that TBK1 strongly interacted with CALCOCO2 at 12 h post-SeV infection, while the apparent interaction between TBK1 and GABARAP could be detected at a later time point (around 24 h post infection) (Figure S5C, S5D), which revealed that CALCOCO2 and GABARAP target TBK1 through different interaction patterns during viral infection.



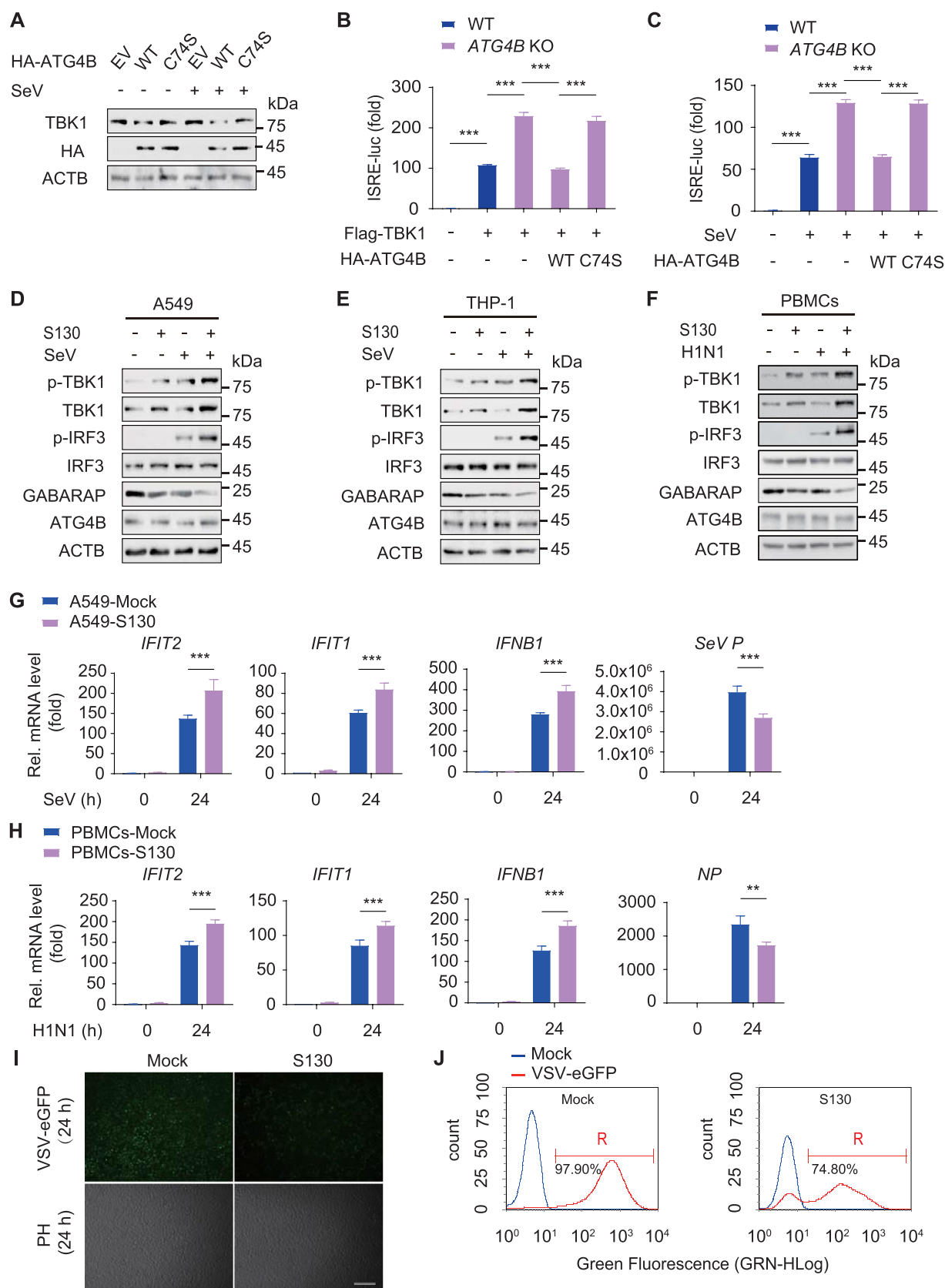


**Figure 6.** ATG4B inhibitor S130 enhances TBK1-centered type I IFN activation. **(A)** Protein lysates of 293T cells transfected with vectors for wild-type (WT) HA-ATG4B or HA-ATG4B<sup>C74S</sup> mutant, followed by treated with SeV (MOI=0.1) infection for 24 h, were immunoblotted with the indicated antibodies. **(B)** Luciferase activity in WT or ATG4B knock-out (KO) 293T cells transfected with an ISRE luciferase reporter (ISRE-luc), together with vector for Flag-TBK1 along with WT HA-ATG4B or HA-ATG4B<sup>C74S</sup> mutant. **(C)** Luciferase activity in WT or ATG4B KO 293T cells transfected with an ISRE-luc, together with vector for WT HA-ATG4B or HA-ATG4B<sup>C74S</sup> mutant, followed by treated with SeV (MOI=0.1) infection for 24 h. **(D)** Protein lysates of A549 cells infected SeV (MOI=0.1) for 24 h, were harvested after S130 (20  $\mu$ M) treatment (6 h) for immunoblot analyses with indicated antibodies. **(E)** Protein lysates of THP-1-derived macrophages infected with SeV (MOI=0.1) for 24 h, were harvested after S130 (20  $\mu$ M) treatment (6 h) for immunoblot analyses with indicated antibodies. **(F)** Protein lysates of human peripheral blood mononuclear cells

In addition, we found that ATG4B could still promote the degradation of TBK1 in *CALCOCO2*-deficient cells (Figure S5E, S5F). Taken together, these results reveal that autophagy subtly modulates TBK1 stability through distinct pathways during the whole process of viral infection.

### ATG4B inhibitor S130 enhances TBK1-centered type I IFN activation

As ATG4B is a cysteine protease, we next to investigate whether the protease activity of ATG4B is required to mediate the autophagic degradation of TBK1. We generated the ATG4B<sup>C74S</sup> mutant with defective protease activity and found that ATG4B<sup>C74S</sup> mutant failed to promote the degradation of TBK1 in both un-infected and infected cells (Figure 6A and S6A). In addition, we found that ATG4B<sup>C74S</sup> mutant could not inhibit the activation of luciferase reporter induced by TBK1 or SeV infection in ATG4B-deficient cells (Figure 6B,C). These results demonstrate that the protease activity of ATG4B is needed for ATG4B-mediated TBK1 degradation.

To further validate the role of ATG4B activity in TBK1 stability, we assessed the effect of ATG4B activity on TBK1 degradation with ATG4B inhibitor, S130, which has high potency and selectivity for ATG4B [29]. Immunoblot analyses revealed that S130 treatment could increase the protein levels of TBK1, as well as phosphorylation of TBK1 and IRF3 in A549 cells (Figure 6D and S6B). This result was further confirmed in THP-1-derived macrophages treated with S130 (Figure 6E and S6C). S130 treatment could also increase the protein levels of TBK1 in PBMCs, as well as phosphorylation of TBK1 and IRF3 upon H1N1 infection (Figure 6F and S6D). Moreover, quantitative RT-PCR analyses showed that S130 treatment resulted in more *IFIT2/ISG54*, *IFIT1/ISG56* and *IFNB1* mRNA than control cells during SeV infection (Figure 6G). Consistently, THP-1-derived macrophages treated with S130 showed less SeV replication than control cells (Figure S6E). Compared with control cells, PBMCs treated with S130 showed increased *IFIT2/ISG54*, *IFIT1/ISG56* and *IFNB1* mRNA during H1N1 infection and suppressed the virus replication (Figure 6H). In order to observe VSV replication in S130 treated cells, we infected A549 cells with GFP-tagged VSV and found that S130 treatment led to a significant reduced fluorescence intensity than control cells (Figure 6I). Meanwhile, flow cytometry analyses demonstrated that S130 resulted in considerably decreased percentage of GFP<sup>+</sup> (virus-infected) cells compared with control cells (Figure 6J). Taken together, S130 could be a promising pharmacological target against TBK1-centered immune responses.

### S130 increases antiviral response and inhibits VSV infection in vivo

ATG4B has been reported to regulate intestinal homeostasis and protect mice from inflammatory colitis [30]. Recently, S130 was identified as a negative effector for the growth of colorectal cancer cells through inhibiting the activity of ATG4B *in vivo* [29]. These results suggest a clue that S130 might have efficacy in ATG4B-mediated antiviral response. To investigate the potential effects of S130 in antiviral response *in vivo*, wild type C57BL/6J mice were i.p. injected with S130 at 20 mg/kg per day for 7 days, which was modified by the reported methods [29]. Mice were infected with VSV ( $1 \times 10^8$  pfu/g) via tail vein injection on day 7. Compared to control group, peritoneal macrophages from mice with S130 treatment showed significantly increased protein levels of TBK1 during VSV infection, as well as phosphorylation of TBK1 and IRF3 (Figure 7A,B). Meanwhile, we found that S130 treatment resulted in more *Ifit1* and *Ifnb* mRNA than the control group during VSV infection, and suppressed the VSV load in the lung of mice (Figure 7C). In addition, reduced tissue damage was observed in the lung of S130-treated mice during VSV infection (Figure 7D). These results demonstrate that S130 treatment increased antiviral response and inhibits VSV infection *in vivo*.

### Discussion

As a serine/threonine kinase, TBK1 plays a fundamental role in cellular response and several signaling pathways including cell growth, proliferation, autophagy, and innate immunity [31,32]. The activity and stability of TBK1 are tightly regulated by multiple post-translational modifications [10,33]. In a recent study, we found that TBK1 could be degraded by selective autophagy with the help of cargo receptor CALCOCO2 [11]. Here, we determined that the ATG cysteine protease ATG4B promotes TBK1 degradation in the absence of the cargo receptor CALCOCO2. Our results suggest autophagy might control the TBK1 stability through distinct molecular mechanisms. Interestingly, TBK1 has been reported to regulate autophagy process by targeting various proteins, such as STX17 (syntaxin 17) and cargo receptors (SQSTM1/p62, OPTN, CALCOCO2/NDP52 and TAX1BP1) [34,35]. These clues indicate that TBK1 plays an essential role in the cross-talk of autophagy and immune response, however, the detailed regulatory mechanism underlying the cross-regulation of autophagy and immune response warrant further investigation.

Emerging evidence demonstrates that ATG proteins regulate the antiviral immunity by controlling the important nodes of type I IFN signaling and selective autophagy cargo

---

(PBMCs) infected with H1N1 (MOI=1) for 24 h, were harvested after S130 (20  $\mu$ M) treatment (6 h) for immunoblot analyses with indicated antibodies. (G) Quantitative RT-PCR analyses of indicated gene expression in A549 cells infected with SeV (MOI=0.1) for 24 h, followed by S130 (20  $\mu$ M) treatment (6 h). (H) Quantitative RT-PCR analyses of indicated gene expression in PBMCs infected with H1N1 (MOI=1) for 24 h, followed by S130 (20  $\mu$ M) treatment (6 h). (I and J) Phase-contrast (PH) and fluorescence microscopy analyses (I) or flow cytometry analyses (J) of A549 cells infected with VSV-eGFP (MOI=0.01) infection for 24 h, following by S130 (20  $\mu$ M) treatment (6 h). Scale bars: 200  $\mu$ m. In (B, C, G and H), all error bars, mean values  $\pm$  SEM, *P*-values were determined by unpaired two-tailed Student's *t* test of *n*=3 independent biological experiments, \*\* *P* < 0.01, \*\*\* *P* < 0.001. For (A, D-F, I and J), similar results are obtained from three independent biological experiments.

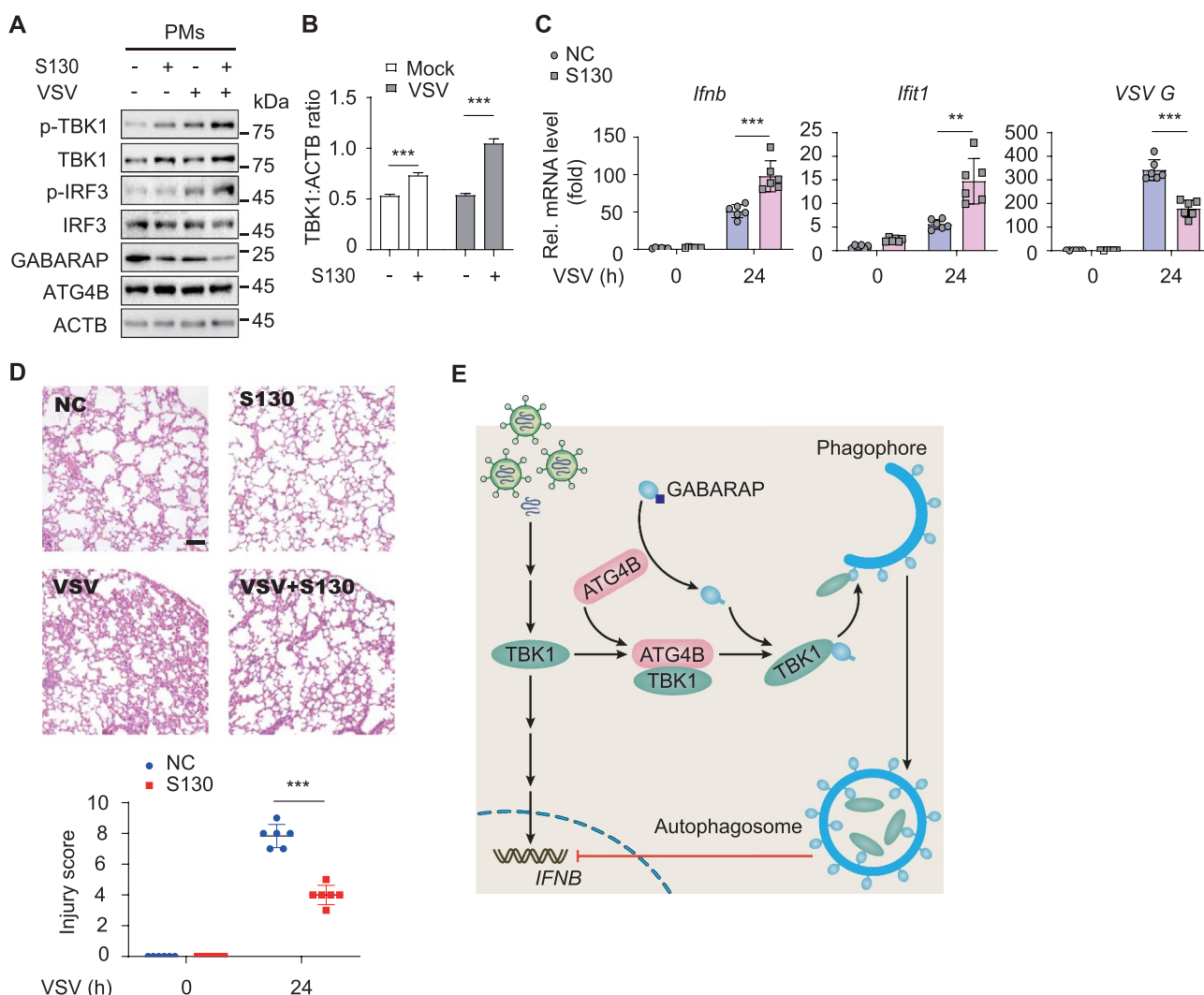


**Figure 7.** S130 augments host antiviral immune response against VSV infection. **(A–D)** C57BL/6J mice (female, 6 weeks old) were randomly divided into 4 groups, 6 mice per group. S130 was administered by i.p. at 20 mg/kg, via intraperitoneal injection from day 0 to day 6. The negative control (NC) and VSV infected (VSV) groups were administered with corn oil via intraperitoneal injection. Mice were infected with VSV ( $1 \times 10^8$  pfu/g) via tail vein injection on day 7. All mice were sacrificed by  $\text{CO}_2$  from compress gas cylinders and assessed at 24 h following the VSV infection. The peritoneal macrophages (PMs) were collected for immunoblot analyses **(A)**. **(B)** Quantification of the expression levels of TBK1 shown in **(A)**. The lung tissues were collected for quantitative RT-PCR analyses **(C)** and hematoxylin-eosin (H&E) staining **(D)**. Scale bar: 100  $\mu\text{m}$ . The lung injury scores per unit of length (mm) of the basement membrane were determined and averaged in six randomly selected nonoverlapping fields from respective individual mouse tissue sections. All histology analyses were conducted in a blinded manner. **(E)** Work model to illustrate how ATG4B negatively regulates TBK1-centered type I interferon (IFN) signaling. In **(B)**, all error bars, mean values  $\pm$  SEM. *P*-values were determined by unpaired two-tailed Student's *t* test of  $n = 3$  independent biological experiments, \*\*\*  $P < 0.001$ . In **(C–D)**, all error bars, mean values  $\pm$  SD. *P*-values were determined by unpaired two-tailed Student's *t* test of  $n = 6$  independent biological mice per group, \*\*  $P < 0.01$ , \*\*\*  $P < 0.001$ . For **(A)**, similar results are obtained from three independent biological experiments.

receptors target intracellular antiviral signaling platforms for degradation to modulate antiviral immune response [36]. ATG5-ATG12 binds to the CARD of RIGI and disrupts RIGI-MAVS interaction to negatively regulates type I IFN signaling. BECN1 suppresses RIGI-MAVS assembly by targeting the CARD of MAVS [37]. Autophagy proteins (such as BECN1, ATG4B, ATG5 and ATG12) have been found to be required for initiation of hepatitis C virus (HCV) proliferation [38]. In addition, *ATG4B* depletion is reported to attenuate EV71 proliferation in EV71 replication step [26]. Here, we identified ATG4B as a negative regulator in antiviral immunity through mediating the autophagic degradation of TBK1. Our results showed that *ATG4B* deficiency markedly increased the TBK1-centered antiviral immunity and suppressed the load of

viruses (such as SeV, VSV and H1N1) in host cells. Our results unravel the physiological significance of ATG4B in modulating the TBK1-centered antiviral immunity response and identify ATG4B as a promising therapeutic target against viral infection.

ATG4B is known to be an Atg8-family protein-processing protein in autophagy. Here, we found that ATG4B serves as a specific adaptor in TBK1-GABARAP association. Overexpression of ATG4B considerably enhanced the interaction between TBK1 and GABARAP, but *ATG4B* depletion abrogated this association. Typically, autophagy cargo receptors and adaptors interact with the LIR docking site (LDS) of mammalian Atg8-family proteins via specialized LIR motifs [15]. LIR-Atg8-family protein interaction is highly selective

for specific Atg8 paralogs (MAP1LC3A, MAP1LC3B, MAP1LC3C and GABARAP, GABARAPL1, GABARAPL2) [39]. We observed a LIR motif was present in ULD domain of TBK1 and found that TBK1 bind to GABARAP via LIR-Atg8 interaction. ATG4B functions as a scaffold to bridge TBK1 to GABARAP. ATG4B-mediated cleavage of GABARAP is essential for the autophagic degradation of TBK1, although the cleavage of GABARAP is not required for its interaction with TBK1. Interestingly, TBK1 is reported to phosphorylate MAP1LC3C and GABARAPL2 to prevent Atg8-family protein delipidation and autophagosome shedding by ATG4 [40], which might form a positive feedback loop to promote TBK1 degradation. These findings suggest that TBK1-Atg8 interaction plays distinct roles in cellular homeostasis and innate immunity by subtly orchestrating diverse molecular pathways.

Autophagy regulation has attracted considerable attention as one of the promising therapeutics strategies for autophagy-related diseases, such as neurodegenerative diseases, cancer, and diabetes [13]. Autophagy inhibition with applicability of autophagy inhibitors is a novel approach for the clinical research [41]. Lysosomal inhibitors, such as CQ and hydroxychloroquine (HCQ), which decrease autophagosome-lysosome fusion, have been used to treat tumors in clinical trials [42]. However, beyond the disposal of autophagosomes, CQ and HCQ also inhibit the degradation of endosomes and vesicular trafficking [43]. Considering the global autophagy inhibitors usually result in cellular disorders and demise, the applicability of specific autophagy inhibitors targeting specific types and steps of autophagic process becomes very important. In the present study, we found that S130, a high potency and selectivity for ATG4B and inhibitor for autophagy flux [29], has a novel role in positive regulation of antiviral immune response. S130 treatment inhibits ATG4B-mediated TBK1 degradation through blocking ATG4B activity. S130 treatment specifically increased the activation of TBK1-centered type I IFN signaling, as well as antiviral immunity response. Moreover, S130 treatment significantly increases antiviral response and inhibits VSV infection *in vivo*. Recently, another ATG4B inhibitor, azalomycin F4a, has been reported to significantly suppress tumor growth and gastric cancer cell invasion through its inhibition of ATG4B [44]. Interestingly, CQ and HCQ have also been reported to show potential antiviral activity upon viral infection [45]. Therefore, develop specific autophagy inhibitors can provide potential therapeutic targets for tumors and host defense against viruses in the future clinical trials.

Collectively, our study reveals a specific role of autophagy-related protein ATG4B in antiviral immune response, and sheds new light on the exploitation of a small-molecule compound to target autophagy process against insufficient immune responses. At the advanced stage of virus infection, ATG4B serves as an adaptor that bridges TBK1 to GABARAP. TBK1 interacts with the GABARAP through its LIR motif. TBK1-GABARAP interaction results in the autophagic degradation of TBK1 (Figure 7E). Moreover, pharmacological ATG4B inhibitor, S130, inhibits ATG4B-dependent autophagic degradation of TBK1 and increases

antiviral response to attenuate viral infection both *in vitro* and *in vivo*. Taken together, we demonstrate that ATG4B is a promising target for antiviral therapy and S130 seems to be a specific potential autophagy inhibitor against virus defense.

## Materials and methods

### Cell lines and culture conditions

HEK293T (GNHu17), A549 (TCHu150) and THP-1 (TCHu57) cells were obtained from the Cell Bank of the Chinese Academy of Sciences. HEK293T and A549 cells were maintained in DMEM medium (Corning, 10-013-CVR) with 10% (vol:vol) fetal bovine serum (Gibco, 10099141) and 1% L-glutamine (Gibco, 35050061). THP-1 cells were maintained in RPMI 1640 medium (Gibco, C22400500BT) with 10% (vol:vol) fetal bovine serum and 1% L-glutamine. THP-1 cells were differentiated into macrophages cultured with RPMI 1640 containing 100 ng/ml phorbol-12-myristate-13-acetate (PMA; Sigma, P8139) for 12 h, and then the macrophages had a resting period of 24 h before being stimulated. Peripheral blood samples from healthy individuals were collected at the Institutional Review Board of The First Affiliated Hospital, Sun Yat-sen University, with ethics approval number [2017]303. Human peripheral blood mononuclear cells (PBMCs) were isolated from the blood of healthy donors. The use of PBMCs was in compliance with institutional ethics guidelines and approved protocols of Sun Yat-sen University. PBMCs were maintained in RPMI-1640 medium (Gibco) 10% fetal bovine serum. All cells were incubated at 37°C incubator with 5% CO<sub>2</sub>.

### Animals

C57BL/6J mice (GDMLAC-O7) were purchased from Guangzhou Medical Laboratory Animal Center of China. Animals were kept and bred in a specific-pathogen free (SPF) environment with standard conditions of temperature (20–26°C) and humidity (40–70%) under a strict 12 h light cycle (lights on at 08:00 a.m. and off 08:00 p.m.) at Sun Yat-sen University, approved all the experimental protocols concerning the handling of mice. All animal experiments protocols were approved by the Animal Care Committee of the Sun Yat-sen University (Authorization number: SYSU-IACUC-2019-B579, Guangzhou, China). The mice were euthanized by CO<sub>2</sub> from compressed gas cylinders, and we complied with all the ethical regulation.

### Plasmids and transfection

Plasmids for ATG4B and its mutant were cloned into the pcDNA3.1 vector (provided by Rongfu Wang laboratory) for transient expression. HEK293T transfection was performed using Lipofectamine 2000 (Invitrogen, 11668019) according to procedures recommended by the manufacturer. Chemically synthesized 21-nucleotide siRNA duplexes were obtained from Sangon and transfected using Lipofectamine RNAiMAX (Invitrogen, 13778150) according to the



manufacturer's instructions. The sequences of target siRNAs were previously reported as follows [44,46]:

SiATG4B-1: 5'-GAAAGAUUCGACUCAGAATT-3';  
 SiATG4B-2: 5'-GGUGUGGACAGAUGAUCUUUGTT-3';  
 SiATG4B-3: 5'-GGUGUGGACAGAUGAUCUUUG-3';  
 Scrambled siRNA: 5'-UUCUCCGAACGUGUCACGUTT-3'.

### Protein degradation inhibition assays

MG132 (10  $\mu$ M) was used to inhibit proteasome-mediated protein degradation. 3 MA (10 mM), CQ (50  $\mu$ M), bafilomycin A1 (Baf A1) (0.2  $\mu$ M) or NH<sub>4</sub>Cl (20 mM) was used to inhibit autolysosome- or lysosome-mediated protein degradation.

### Antibodies and reagents

Monoclonal anti-Flag M2-peroxidase (A8592), monoclonal anti-ACTB/ $\beta$ -actin antibody produced in mouse AC-74 (A2228), and anti-Flag M2 affinity gel (A2220) were purchased from Sigma. Anti-MYC-horseradish peroxidase (11814150001) and anti-HA-peroxidase (high affinity from rat immunoglobulin G1) (12013819001) were purchased from Roche. BECN1/Beclin-1 antibody (3738 S), TBK1/NAK antibody (3013 S), phospho-TBK1/NAK (Ser172, D52C2) rabbit mAb (5483 S), and phospho-IRF3 (Ser396, 4D4G) rabbit mAb (4947 S) were purchased from Cell Signaling Technology. IRF3 antibody (FL-425) (sc-9082) and TBK1 antibody (L-15) (sc-9910) were purchased from Santa Cruz Biotechnology. ATG4B polyclonal antibody (15131-1-AP), ATG16L1 polyclonal antibody (19812-1-AP), CALCOCO2 polyclonal antibody (12229-1-AP), and GABARAP polyclonal antibody (18723-1-AP) were purchased from Proteintech Group. Alexa Fluor 488 goat anti-Rabbit IgG (H+L) (A-11034) was purchased from Thermofisher. CF568 donkey anti goat IgG (H+L) (20106-1) was purchased from Biotium. S130 is obtained from chemical synthesis as previously described [29].

### Generation of knockout cell lines

For ATG4B knockout cells, lentiviral particles were produced by transfecting HEK293T cells with target sequences cloned into pLentiCRISPRv2 (Addgene, 52961; deposited by Jun Cui). The medium was changed the following day and the viral containing supernatant was collected 48 h after transfection, filtered through a 0.45- $\mu$ m filter and subsequently used to infect cells with polybrene (8  $\mu$ g/mL; Sigma, 107689). 293T cells were infected by incubation with lentivirus-containing supernatant for 48 h. To generate ATG4B and GABARAP knockout cells, the target sequence (ATG4B guide: 5'-CACCGGCCTAGGTGCCGGCACACCA-3'; GABARAP guide: 5'-CACCGAGGTCTCCTATCCGAGCTTT-3') were cloned into pLentiCRISPRv2 by cutting with BsmBI. Infected cells were treated with 1  $\mu$ g/mL puromycin for 48 h to enrich transfected cells, which were then diluted and placed into 96-well plates for single colonies. The gRNAs for BECN1, CALCOCO2 and TBK1 were previously reported [37,47].

### Immunoprecipitation and immunoblot analyses

For immunoprecipitation, whole-cell extracts were prepared after transfection or stimulation with appropriate ligands, followed by incubation overnight with the appropriate antibodies plus protein A/G beads (Pierce, 20423) or anti-Flag (Sigma, A2220). Beads were then washed five times with low-salt lysis buffer (50 mM HEPES, pH 7.5 [Gibco, 15630080], 150 mM NaCl [Sigma, S5886], 1 mM EDTA [Vetec, 60-00-4], 10% glycerol [Vetec, V900122], 1.5 mM MgCl<sub>2</sub> [Vetec, V900020], 1% Triton X-100 [Sigma, T9284]), and immunoprecipitates were eluted with 2 $\times$ SDS Loading Buffer (FD Biotechnology, FD003) and resolved by SDS-PAGE. Proteins were transferred to PVDF membranes (Bio-Rad, 1620177) and further incubated with the appropriate antibodies. Immobilon Western Chemiluminescent HRP Substrate (Millipore, WBKLS0500) was used for protein detection.

### Fluorescence microscopy

Cells were cultured on glass bottom culture dishes (Nest Scientific, 801002) and directly observed as previously described [48]. For examination by immunofluorescence microscopy, cells were fixed with 4% paraformaldehyde for 15 min, and then permeabilized in methyl alcohol for 10 min at -20°C. After washing with PBS for three times, cells were blocked in 5% fetal goat serum (Boster Biological, AR1009) for 1 h, and then incubated with primary antibodies diluted in 10% bull serum albumin (Sigma, A1933) overnight. The cells were washed, and followed by a fluorescently labeled secondary antibody. Confocal images were examined using a Leica TCS-SP8 confocal microscope (TCS-SP8, Leica) equipped with a  $\times$ 100 NA oil-immersion objective.

### Virus infection

Human influenza virus A/Puerto Rico/8/34 (H1N1) (PR8) was kindly provided by Dr. Hui Zhang and Dr. Yi-Ping Li (Zhongshan Medical School, Sun Yat-sen University). SeV and VSV-eGFP were kindly provided by Dr. Xiaofeng Qin (Suzhou Institute of Systems Medicine). H1N1, SeV and VSV-eGFP were titered on Vero cells. Virus titers were measured by means of 50% of the tissue culture's infectious dose (TCID<sub>50</sub>). For *in vivo* studies, C57BL/6J mice (female, 6 weeks old) were randomly divided into 4 groups, 6 mice per group. S130 was administered by i.p. at 20 mg/kg, via intraperitoneal injection from day 0 to day 6. The negative control (NC) and VSV infected (VSV) groups were administered with corn oil via intraperitoneal injection. Mice were infected with VSV (1 $\times$ 10<sup>8</sup> pfu/g) via tail vein injection on day 7. All mice were sacrificed by CO<sub>2</sub> from compress gas cylinders and assessed at 24 h following the VSV infection. The peritoneal macrophages (PMs) were collected for immunoblot analyses, the lung tissues were collected for hematoxylin-eosin (H&E) staining and quantitative RT-PCR analyses.

### Quantitative RT-PCR

Total RNA was extracted from cells using the Trizol reagent (Invitrogen, 10296010) according to the manufacturer's instructions. For RT-PCR analyses, cDNA was generated with HiScript-III RT SuperMix for qPCR (+gDNA wiper) (Vazyme, R323-01) and was analyzed by quantitative real-time PCR using the 2× PolarSignal™ SYBR Green mix Taq (MIK, MKG900-10). The sequences of primers are as follows:

Human *IFNB1* forward: 5'-GATGAACTTTGACATCCCTGAG-3',  
 Human *IFNB1* reverse: 5'-TCAACAATAGTCTCATTCCAGC-3';  
 Human *IFIT2* forward: 5'-TATTGGTGCCAGAAGAGGAAGA-3',  
 Human *IFIT2* reverse: 5'-CAGGTGAAATGGCATTCTTAGTT-3';  
 Human *IFIT1* forward: 5'-TCAGGTCAAGGATAGTCTGGAG-3',  
 Human *IFIT1* reverse: 5'-AGGTTGTGATTCCCACACTGTA-3';  
 Human *TBK1* forward: 5'-TCATCTTAGGAAACAGTTAT-3',  
 Human *TBK1* reverse: 5'-GTAAACATTTTCTGAGGC-3';  
 Human *ATG4B* forward: 5'-GGTGTGGACAGATGATCTTTGC-3',  
 Human *ATG4B* reverse: 5'-CCAACCTCCATTTGCGCTATC-3';  
 Human *RPL13A* forward: 5'-GCCATCGTGGCTAAACAGGTA-3',  
 Human *RPL13A* reverse: 5'-GTTGGTGTTCATCCGCTTGC-3';  
 Mouse *Ifnb* forward: 5'-AACCTCACCTACAGGGCGGACTTCA-3',  
 Mouse *Ifnb* reverse: 5'-TCCCACGTCAATCTTTCTCTTGTCTTT-3';  
 Mouse *Ifit1* forward: 5'-CAGCAGCACATCTTGCCAAA-3',  
 Mouse *Ifit1* reverse: 5'-GAGGAAGGTGATGCCTGCAA-3';  
 Mouse *Gapdh* forward: 5'-TCAAGCTCATTTCCTGGTATGACA-3',  
 Mouse *Gapdh* reverse: 5'-TAGGGCCTCTCTTGCTCAGT-3';  
 SeV *P* forward: 5'-TGTTATCGGATTCCCTCGACGCAGTC-3',  
 SeV *P* reverse: 5'-TACTCTCCTCACCTGATCGATTATC-3';  
 H1N1 *NP* forward: 5'-TGTGTATGGACCTGCCGTAGC-3',  
 H1N1 *NP* reverse: 5'-CCATCCACACCAGTTGACTCTTG-3'.

### Luciferase and reporter assays

Cells were plated in 24-well plates and transfected with plasmids encoding the ISRE luciferase reporter (firefly luciferase, 30 ng) and pRL-TK (Renilla luciferase, 10 ng), which were kindly provided by Dr. Rong-Fu Wang (Houston Methodist Research

Institute), together with different plasmids (100 ng). Cells treated with SeV or IC poly (I: C) stimulation for the indicated times were collected and luciferase activity was measured with Dual-Luciferase Assay (Promega, E1910) with a Luminoskan Ascent luminometer (Thermo Fisher Scientific). Reporter gene activity was determined by normalization of the firefly luciferase activity to Renilla luciferase activity. The values were means ± SEM of 3 independent experiments.

### Histological assessment

The mice were euthanized by CO<sub>2</sub> from compressed gas cylinders. Then the tissues were removed and fixed in 4% paraformaldehyde (Meilunbio, MA0192) for more than 24 h, and embedded in paraffin. The sections (thickness, 6 μm) were stained with hematoxylin & eosin (Meilunbio, MB9898). The lung injury scores per unit of length (mm) of the basement membrane were determined and averaged in six randomly selected nonoverlapping fields from respective individual mouse tissue sections using a microscope (Eclipse Ni-U; Nikon) and all histology analyses for H&E staining were conducted in a blinded manner as a combination of tissue damage (score 0–5) and inflammatory cell infiltration (score 0–5) with a total ranging from 0 to 10.

### Statistical analyses

Data are represented as mean ± SEM unless otherwise indicated, and Student's *t*-test was used for all statistical analyses with the GraphPad Prism 8 software. Differences between two groups were considered significant when *P* value was less than 0.05.

### Disclosure statement

No potential conflict of interest was reported by the authors.

### Funding

This work was supported by the National Natural Science Foundation of China (32170876, 31970700, 32270922, 92042303, 31970538 and 31870862), Science and Technology Planning Project of Guangzhou, China (201907010038), Guangdong Basic and Applied Basic Research Foundation (2020B1515120090), and the Fundamental Research Funds for the Central Universities, Sun Yat-sen University (22qntd2601 and 23lgbj012), Plan on enhancing scientific research in GMU (02-410-2302269XM), National Key R&D Program of China (2021YFA0805800 and 2020YFA0803202), the Guangzhou Medical University Discipline Construction Funds (Basic Medicine) (JCXKJS2022A02), the 111 Project (D18010), the Local Innovative and Research Teams Project of Guangdong Pearl River Talents Program (2017BT01S155).

### ORCID

Min Li  <http://orcid.org/0000-0002-5657-8675>

Shouheng Jin  <http://orcid.org/0000-0002-2728-2859>

### References

- [1] Wang J, Flavell RA, Li HB. Antiviral immunity: a link to bile acids. *Cell Res.* 2019;29(3):177–178. doi: 10.1038/s41422-019-0148-5

- [2] Chow KT, Gale M, Loo YM. RIG-I and other RNA sensors in antiviral immunity. In: Littman D, and Yokoyama W, editors. *Annual Review of Immunology*. 2018;36:667–694. doi: [10.1146/annurev-immunol-042617-053309](https://doi.org/10.1146/annurev-immunol-042617-053309)
- [3] Rehwinkel J, Gack MU. RIG-I-like receptors: their regulation and roles in RNA sensing. *Nat Rev Immunol*. 2020;20(9):537–551. doi: [10.1038/s41577-020-0288-3](https://doi.org/10.1038/s41577-020-0288-3)
- [4] Hur S. Double-stranded RNA sensors and modulators in innate immunity. *Annu Rev Immunol*. 2019;37:349–375. doi: [10.1146/annurev-immunol-042718-041356](https://doi.org/10.1146/annurev-immunol-042718-041356)
- [5] Liu J, Qian C, Cao X. Post-translational modification control of innate immunity. *Immunity*. 2016;45(1):15–30. doi: [10.1016/j.immuni.2016.06.020](https://doi.org/10.1016/j.immuni.2016.06.020)
- [6] VV S, Niedenthal R, Pich A, et al. SUMO modification of TBK1 at the adaptor-binding C-terminal coiled-coil domain contributes to its antiviral activity. *Biochim Biophys Acta*. 2015;1853:136–143. doi: [10.1016/j.bbamcr.2014.10.008](https://doi.org/10.1016/j.bbamcr.2014.10.008)
- [7] Li X, Zhang Q, Ding Y, et al. Methyltransferase Dnmt3a upregulates HDAC9 to deacetylate the kinase TBK1 for activation of antiviral innate immunity. *Nat Immunol*. 2016;17(7):806–815. doi: [10.1038/ni.3464](https://doi.org/10.1038/ni.3464)
- [8] Cui J, Li Y, Zhu L, et al. NLRP4 negatively regulates type I interferon signaling by targeting the kinase TBK1 for degradation via the ubiquitin ligase DTX4. *Nat Immunol*. 2012;13(4):387–395. doi: [10.1038/ni.2239](https://doi.org/10.1038/ni.2239)
- [9] Zheng Q, Hou J, Zhou Y, et al. Siglec1 suppresses antiviral innate immune response by inducing TBK1 degradation via the ubiquitin ligase TRIM27. *Cell Res*. 2015;25(10):1121–1136. doi: [10.1038/cr.2015.108](https://doi.org/10.1038/cr.2015.108)
- [10] Deng M, Tam JW, Wang L, et al. TRAF3IP3 negatively regulates cytosolic RNA induced anti-viral signaling by promoting TBK1 K48 ubiquitination. *Nat Commun*. 2020;11(1):2193. doi: [10.1038/s41467-020-16014-0](https://doi.org/10.1038/s41467-020-16014-0)
- [11] Xie W, Jin S, Zhang C, et al. Selective autophagy controls the stability of TBK1 via NEDD4 to balance host defense. *Cell Death Differ*. 2022;29(1):40–53. doi: [10.1038/s41418-021-00833-9](https://doi.org/10.1038/s41418-021-00833-9)
- [12] Zhao X, Di Q, Yu J, et al. USP19 (ubiquitin specific peptidase 19) promotes TBK1 (TANK-binding kinase 1) degradation via chaperone-mediated autophagy. *Autophagy*. 2022;18(4):891–908. doi: [10.1080/15548627.2021.1963155](https://doi.org/10.1080/15548627.2021.1963155)
- [13] Levine B, Kroemer G. Biological functions of autophagy genes: a disease perspective. *Cell*. 2019;176(1–2):11–42. doi: [10.1016/j.cell.2018.09.048](https://doi.org/10.1016/j.cell.2018.09.048)
- [14] Deretic V, Levine B. Autophagy balances inflammation in innate immunity. *Autophagy*. 2018;14(2):243–251. doi: [10.1080/15548627.2017.1402992](https://doi.org/10.1080/15548627.2017.1402992)
- [15] Deretic V. Autophagy in inflammation, infection, and immunometabolism. *Immunity*. 2021;54(3):437–453. doi: [10.1016/j.immuni.2021.01.018](https://doi.org/10.1016/j.immuni.2021.01.018)
- [16] Jang YJ, Kim JH, Byun S. Modulation of autophagy for controlling immunity. *Cells*. 2019;8(2):138. doi: [10.3390/cells8020138](https://doi.org/10.3390/cells8020138)
- [17] Choi Y, Bowman JW, Jung JU. Autophagy during viral infection - a double-edged sword. *Nat Rev Microbiol*. 2018;16:341–354. doi: [10.1038/s41579-018-0003-6](https://doi.org/10.1038/s41579-018-0003-6)
- [18] Huang L, Yue J. The interplay of autophagy and enterovirus. *Semin Cell Dev Biol*. 2020;101:12–19. doi: [10.1016/j.semcdb.2019.08.001](https://doi.org/10.1016/j.semcdb.2019.08.001)
- [19] Taylor MP, Kirkegaard K. Modification of cellular autophagy protein LC3 by poliovirus. *J Virol*. 2007;81(22):12543–12553. doi: [10.1128/JVI.00755-07](https://doi.org/10.1128/JVI.00755-07)
- [20] Jackson WT, Giddings TH Jr., Taylor MP, et al. Subversion of cellular autophagosomal machinery by RNA viruses. *PLoS Biol*. 2005;3(5):e156. doi: [10.1371/journal.pbio.0030156](https://doi.org/10.1371/journal.pbio.0030156)
- [21] Ichimura Y, Kirisako T, Takao T, et al. A ubiquitin-like system mediates protein lipidation. *Nature*. 2000;408(6811):488–492. doi: [10.1038/35044114](https://doi.org/10.1038/35044114)
- [22] Yang G, Li Y, Zhao Y, et al. Targeting Atg4B for cancer therapy: Chemical mediators. *Eur J Med Chem*. 2021;209:112917. doi: [10.1016/j.ejmech.2020.112917](https://doi.org/10.1016/j.ejmech.2020.112917)
- [23] Li M, Hou Y, Wang J, et al. Kinetics comparisons of mammalian Atg4 homologues indicate selective preferences toward diverse Atg8 substrates. *J Biol Chem*. 2011;286(9):7327–7338. doi: [10.1074/jbc.M110.199059](https://doi.org/10.1074/jbc.M110.199059)
- [24] Agrotis A, Pengo N, Burden JJ, et al. Redundancy of human ATG4 protease isoforms in autophagy and LC3/GABARAP processing revealed in cells. *Autophagy*. 2019;15(6):976–997. doi: [10.1080/15548627.2019.1569925](https://doi.org/10.1080/15548627.2019.1569925)
- [25] Hait AS, Olagnier D, Sancho-Shimizu V, et al. Defects in LC3B2 and ATG4A underlie HSV2 meningitis and reveal a critical role for autophagy in antiviral defense in humans. *Sci Immunol*. 2020;5(54): doi: [10.1126/sciimmunol.abc2691](https://doi.org/10.1126/sciimmunol.abc2691)
- [26] Sun Y, Zheng Q, Wang Y, et al. Activity-based protein profiling identifies ATG4B as a key host factor for enterovirus 71 proliferation. *J Virol*. 2019;93(24): doi: [10.1128/JVI.01092-19](https://doi.org/10.1128/JVI.01092-19)
- [27] Tian Y, Wang ML, Zhao J. Crosstalk between autophagy and type I interferon responses in innate antiviral immunity. *Viruses*. 2019;11(2):11. doi: [10.3390/v11020132](https://doi.org/10.3390/v11020132)
- [28] Kabeya Y, Mizushima N, Yamamoto A, et al. LC3, GABARAP and GATE16 localize to autophagosomal membrane depending on form-II formation. *J Cell Sci*. 2004;117(13):2805–2812. doi: [10.1242/jcs.01131](https://doi.org/10.1242/jcs.01131)
- [29] Fu Y, Hong L, Xu J, et al. Discovery of a small molecule targeting autophagy via ATG4B inhibition and cell death of colorectal cancer cells in vitro and in vivo. *Autophagy*. 2019;15(2):295–311. doi: [10.1080/15548627.2018.1517073](https://doi.org/10.1080/15548627.2018.1517073)
- [30] Cabrera S, Fernández AF, Mariño G, et al. Atg4b/autophagin-1 regulates intestinal homeostasis and protects mice from experimental colitis. *Autophagy*. 2013;9:1188–1200. doi: [10.4161/auto.24797](https://doi.org/10.4161/auto.24797)
- [31] Weil R, Laplantine E, Génin P. Regulation of TBK1 activity by Optineurin contributes to cell cycle-dependent expression of the interferon pathway. *Cytokine Growth Factor Rev*. 2016;29:23–33. doi: [10.1016/j.cytogfr.2016.03.001](https://doi.org/10.1016/j.cytogfr.2016.03.001)
- [32] Alam M, Ansari MM, Noor S, et al. Therapeutic targeting of TANK-binding kinase signaling towards anticancer drug development: Challenges and opportunities. *Int j biol macromol*. 2022;207:1022–1037. doi: [10.1016/j.ijbiomac.2022.03.157](https://doi.org/10.1016/j.ijbiomac.2022.03.157)
- [33] Zhao C, Zhao W. TANK-binding kinase 1 as a novel therapeutic target for viral diseases. *Expert Opin Ther Targets*. 2019;23(5):437–446. doi: [10.1080/14728222.2019.1601702](https://doi.org/10.1080/14728222.2019.1601702)
- [34] Kumar S, Gu Y, Abudu YP, et al. Phosphorylation of Syntaxin 17 by TBK1 controls autophagy initiation. *Dev Cell*. 2019;49:130–144.e136. doi: [10.1016/j.devcel.2019.01.027](https://doi.org/10.1016/j.devcel.2019.01.027)
- [35] Richter B, Sliter DA, Herhaus L, et al. Phosphorylation of OPTN by TBK1 enhances its binding to Ub chains and promotes selective autophagy of damaged mitochondria. *Proc Natl Acad Sci U S A*. 2016;113(15):4039–4044. doi: [10.1073/pnas.1523926113](https://doi.org/10.1073/pnas.1523926113)
- [36] Viret C, Duclaux-Loras R, Nancey S, et al. Selective autophagy receptors in antiviral defense. *Trends Microbiol*. 2021;29(9):798–810. doi: [10.1016/j.tim.2021.02.006](https://doi.org/10.1016/j.tim.2021.02.006)
- [37] Jin S, Tian S, Chen Y, et al. USP19 modulates autophagy and antiviral immune responses by deubiquitinating Beclin-1. *Embo J*. 2016;35(8):866–880. doi: [10.15252/embj.201593596](https://doi.org/10.15252/embj.201593596)
- [38] Dreux M, Gastaminza P, Wieland SF, et al. The autophagy machinery is required to initiate hepatitis C virus replication. *Proc Natl Acad Sci U S A*. 2009;106(33):14046–14051. doi: [10.1073/pnas.0907344106](https://doi.org/10.1073/pnas.0907344106)
- [39] Wirth M, Mouilleron S, Zhang W, et al. Phosphorylation of the LIR Domain of SCOC modulates atg8 binding affinity and specificity. *J Mol Biol*. 2021;433(13):166987. doi: [10.1016/j.jmb.2021.166987](https://doi.org/10.1016/j.jmb.2021.166987)
- [40] Herhaus L, Bhaskara RM, Lystad AH, et al. TBK1-mediated phosphorylation of LC3C and GABARAP-L2 controls autophagosome shedding by ATG4 protease. *EMBO Rep*. 2020;21:e48317. doi: [10.15252/embr.201948317](https://doi.org/10.15252/embr.201948317)
- [41] Galluzzi L, Bravo-San Pedro JM, Levine B, et al. Pharmacological modulation of autophagy: therapeutic potential and persisting obstacles. *Nat Rev Drug Discov*. 2017;16(7):487–511. doi: [10.1038/nrd.2017.22](https://doi.org/10.1038/nrd.2017.22)

- [42] Mauthe M, Orhon I, Rocchi C, et al. Chloroquine inhibits autophagic flux by decreasing autophagosome-lysosome fusion. *Autophagy*. 2018;14(8):1435–1455. doi: [10.1080/15548627.2018.1474314](https://doi.org/10.1080/15548627.2018.1474314)
- [43] Rodriguez-Boulan E, Kreitzer G, Müsch A. Organization of vesicular trafficking in epithelia. *Nat Rev Mol Cell Biol*. 2005;6(3):233–247. doi: [10.1038/nrm1593](https://doi.org/10.1038/nrm1593)
- [44] Zhong L, Yang B, Zhang Z, et al. Targeting autophagy peptidase ATG4B with a novel natural product inhibitor Azalomycin F4a for advanced gastric cancer. *Cell Death Dis*. 2022;13(2):161. doi: [10.1038/s41419-022-04608-z](https://doi.org/10.1038/s41419-022-04608-z)
- [45] Bakadia BM, He F, Souho T, et al. Prevention and treatment of COVID-19: Focus on interferons, chloroquine/hydroxychloroquine, azithromycin, and vaccine. *Biomed Pharmacother*. 2021;133:111008. doi: [10.1016/j.biopha.2020.111008](https://doi.org/10.1016/j.biopha.2020.111008)
- [46] Sun L, Xiong H, Chen L, et al. Deacetylation of ATG4B promotes autophagy initiation under starvation. *Sci Adv*. 2022;8(31):eabo0412. doi: [10.1126/sciadv.abo0412](https://doi.org/10.1126/sciadv.abo0412)
- [47] Vargas JNS, Wang C, Bunker E, et al. Spatiotemporal Control of ULK1 Activation by NDP52 and TBK1 during selective autophagy. *Molecular Cell*. 2019;74:347–362. doi: [10.1016/j.molcel.2019.02.010](https://doi.org/10.1016/j.molcel.2019.02.010)
- [48] Chen M, Meng Q, Qin Y, et al. TRIM14 Inhibits cGAS degradation mediated by selective autophagy receptor p62 to promote innate immune responses. *Molecular Cell*. 2016;64(1):105–119. doi: [10.1016/j.molcel.2016.08.025](https://doi.org/10.1016/j.molcel.2016.08.025)